J|A|C|S ARTICLES

Published on Web 09/03/2009

Probing the Dynamics of a Protein Hydrophobic Core by Deuteron Solid-State Nuclear Magnetic Resonance Spectroscopy

Liliya Vugmeyster,*,† Dmitry Ostrovsky,† Joseph J. Ford,‡ Sarah D. Burton,‡ Andrew S. Lipton,‡ Gina L. Hoatson,§ and Robert L. Vold§

University of Alaska—Anchorage, Anchorage, Alaska 99508, Pacific Northwest National Laboratory, Richland, Washington 99354, and College of William and Mary, Williamsburg, Virginia 23187

Received April 14, 2009; E-mail: aflv@uaa.alaska.edu

Abstract: With the goal of investigating dynamical features of hydrophobic cores of proteins over a wide range of temperatures, the chicken villin headpiece subdomain protein (HP36) was labeled at a "single" site corresponding to any one of the two $C^{\delta}D_3$ groups of leucine-69, which is located in a key position of the core. The main techniques employed are deuteron NMR quadrupolar echo line shape analysis, and T_{1Z} (Zeeman) and T_{1Q} (quadrupolar order) relaxation experiments performed at 11.7 and 17.6 T over the temperature range of 112 to 298 K. The experimental data are compared with computer simulations. The deuteron line shapes give an excellent fit to a three-mode motional model that consists of (a) fast three-site rotational jumps about the pseudo C_3 methyl spinning axis, (b) slower reorientation of the spinning axis, described by diffusion along a restricted arc, and (c) large angle jumps between traces of rotameric conformers. Relaxation behavior is described by a phenomenological distribution of activation energies for three-site hops at high temperatures that collapses to a single, distinctly smaller value for lower temperatures.

Introduction

It has been long recognized that protein structures are not static but can rather be viewed as an ensemble of conformations (substates) with somewhat different free energies within the free energy "landscape".[1] Protein dynamics, which are crucial for many biological processes, involve transitions between these substates, as well as small amplitude fluctuations about the equilibrium positions of the substates. The populations of the substates and the rates of transitions between them change as a function of temperature, thus rendering temperature a useful variable to probe the motion. The hydrophobic core of proteins plays a major role in protein stability, folding pathways, and biological function.[2] It is a complex dynamic medium reflecting the existence of conformational ensemble.

Deuteron NMR has been long known as a powerful tool for probing molecular dynamics in various systems such as liquid crystals, synthetic polymers, and biological molecules.[3−6] Deuteron NMR line shapes and relaxation rates are usually dominated by one, single-particle mechanism: the interaction of the nuclear electric quadrupole moment with the electric field gradient at the site of the nucleus. The deuteron has a relatively small electric quadrupole moment, which makes it easy to work with experimentally. Available deuteron NMR techniques cover a very broad range of time scales, from pico- to milliseconds.

Even for soluble proteins the solid phase offers several advantages for dynamics studies by NMR. These include the lack of constraints imposed by protein solubility, the possibility to cover a very broad temperature range, and the absence of contributions from overall molecular tumbling.[6] The latter factor often constrains the range of time scales that can be unambiguously characterized by standard relaxation techniques in solution and requires more complicated methodologies.[7−9] In solid proteins, overall molecular motion is either absent entirely or shifted to much longer time scales. Another advantage of the solid phase is the ability to study the effect of hydration on local segmental dynamics. As a result, many studies have focused on investigations of dynamics by solid-state NMR, examples of which include works by McDermott's,[10,11] Ems-

† University of Alaska—Anchorage.
‡ Pacific Northwest National Laboratory.
§ College of William and Mary.

(1) Onuchic, J. N.; LutheySchulten, Z.; Wolynes, P. G. *Annu. Rev. Phys. Chem.* **1997**, *48*, 545–600.
(2) Creighton, T. E. *Proteins: structures and molecular properties*; W. H. Freeman and Company: New York, 1993.
(3) Vold, R. R. Deuterium NMR studies of dynamics in solids and liquid crystals. In *Nuclear Magnetic Resonance Probes of Molecular Dynamics*; Tycko, R., Ed.; Kluwer Academic Publishers: Dordrecht, 1994; pp 27−112.
(4) Vold, R. L.; Vold, R. R. Deuterium Relaxation in Molecular Solids. In *Advances in Magnetic and Optical Resonance*; Warren, W., Ed.; Academic Press: San Diego, 1991; pp 85−171.
(5) Duer, M. J. *Solid-State NMR Spectroscopy*; Blackwell Publishing Ltd.: Oxford, 2004.
(6) Krushelnitsky, A.; Reichert, D. *Prog. Nucl. Magn. Reson. Spectrosc.* **2005**, *47*, 1–25.
(7) Mittermaier, A.; Kay, L. E. *Science* **2006**, *312*, 224–228.
(8) Palmer, A. G.; Kroenke, C. D.; Loria, J. P. *Methods Enzymol.* **2001**, *339*, 204–238.
(9) Meirovitch, E.; Shapiro, Y. E.; Polimeno, A.; Freed, J. H. *J. Phys. Chem. B* **2007**, *111*, 12865–12875.
(10) Lorieau, J. L.; Day, L. A.; McDermott, A. E *Proc. Natl. Acad. Sci. U.S.A.* **2008**, *105*, 10366–10371.
(11) McDermott, A.; Polenova, T. *Curr. Opin. Struct. Biol.* **2007**, *17*, 617–622.

10.1021/ja902977u CCC: $40.75

ley's,[12] Baldus's,[13] and Skrynnikov/Reif's groups.[14] Closely related to this study are previous works that utilize deuteron NMR spectroscopy to probe biomolecular dynamics.[6,15−23]

Single-site labeling at a key site of a biological molecule allows for a more detailed quantitative analysis than is usually possible in samples with multiple labels. Magic-angle spinning techniques which are used for site-specific resolution are not necessary in this case, and one can thus readily expand the range of temperatures accessible experimentally. The analysis of experimental data is also simplified because of the absence of overlap between the signals and minimal complications arising from spin-diffusion.[24]

The goal of this work is to investigate essential features of the dynamics in a hydrophobic core of a hydrated protein over a wide range of temperatures. We look at chicken villin headpiece subdomain (HP36). HP36 is one of the smallest known examples of a cooperatively folded domain of a naturally occurring protein. The protein is a popular system for computational and experimental protein folding studies.[25−38]

Villin is an F-actin bundling protein involved in the maintenance of the microvilli of the absorptive epithelia.[39,40] The villin headpiece subdomain is a 35-residue, autonomously folding, thermostable motif at the extreme C-terminus of villin.[31] This subdomain spans residues 42−76 (residues 791−825 of intact chicken villin) of the full-length 76 amino acid residue villin headpiece. The recombinant form of the subdomain, HP36, has an additional N-terminal methionine residue designated arbitrarily as residue 41. The structure of HP36, as determined by X-ray and NMR spectroscopy,[41,42] consists of three short helices (residues 44−51, 54−60, and 64−74) surrounding a tightly packed hydrophobic core. Three phenylalanine side chains, F47, F51, F58, form the basis of the core.[25,41,42] All three helices contribute additional residues to the hydrophobic core. Additional core residues which have less than 70% solvent accessibility are L42, V50, A57, Q66, K65, L69, and G74. The third helix is disordered in isolation, whereas the subdomain lacking the third helix retains residual structure.[33] Havlin and Tycko[28] studied local conformational distributions of HP36 by solid-state NMR analyzing the line shapes of C_α/C_β cross-peaks as a function of denaturant concentration in selected residues in each of the helices: V50, A57, and L69. The results showed that L69, which belongs to the third helix, becomes most disordered at high concentrations of denaturant, indicating that the native conformational distribution for this residue is highly dependent on tertiary contacts.

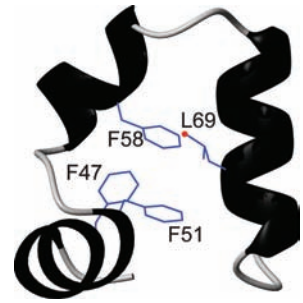

Figure 1. Ribbon diagram of HP36 with the side chains of the key hydrophobic residues in purple. One of the two possible labeled C^δ methyl positions of L69 is shown in red. The amino acid sequence is MLSDED-FKAVFGMTRSAFANLPLWKQQNLKKEKGLF.

Single-site labeling is used in this work to perform a detailed dynamic analysis of a hydrated HP36 sample in solid state. C^δ methyl groups of leucine side chains have been shown to participate not only in methyl rotation but also in a variety of slower motions.[15,18] In order to probe the dynamics of the hydrophobic core of HP36 we obtained a sample with a deuteron label on a leucine C^δ methyl group located at a key position in the core. The label was incorporated randomly into either of the two C^δ methyl groups of L69. Figure 1 shows a ribbon diagram of HP36 with the three phenylalanine side chains and the L69 side chain.

To probe the dynamics, we utilize deuteron line shape analysis, which is sensitive to micro- to millisecond time scales of motions, as well as measurements of T_{1Z}(Zeeman) and T_{1Q}

(12) Giraud, N.; Blackledge, M.; Goldman, M.; Bockmann, A.; Lesage, A.; Penin, F.; Emsley, L. *J. Am. Chem. Soc.* **2005**, *127*, 18190–18201.
(13) Ader, C.; Schneider, R.; Seidel, K.; Etzkorn, M.; Becker, S.; Baldus, M. *J. Am. Chem. Soc.* **2009**, *131*, 170–176.
(14) Agarwal, V.; Xue, Y.; Reif, B.; Skrynnikov, N. R. *J. Am. Chem. Soc.* **2008**, *130*, 16611–16621.
(15) Batchelder, L. S.; Sullivan, C. E.; Jelinski, L. W.; Torchia, D. A. *Proc. Natl. Acad. Sci. U.S.A.* **1982**, *79*, 386–389.
(16) Brown, M. F.; Heyn, M. P.; Job, C.; Kim, S.; Moltke, S.; Nakanishi, K.; Nevzorov, A. A.; Struts, A. V.; Salgado, G. F. J.; Wallat, I. *Biochim. Biophys. Acta Biomembr.* **2007**, *1768*, 2979–3000.
(17) Copie, V.; McDermott, A. E.; Beshah, K.; Williams, J. C.; Spijker-assink, M.; Gebhard, R.; Lugtenburg, J.; Herzfeld, J.; Griffin, R. G. *Biochemistry* **1994**, *33*, 3280–3286.
(18) Keniry, M. A.; Kintanar, A.; Smith, R. L.; Gutowsky, H. S.; Oldfield, E. *Biochemistry* **1984**, *23*, 288–298.
(19) Mack, J. W.; Usha, M. G.; Long, J.; Griffin, R. G.; Wittebort, R. J. *Biopolymers* **2000**, *53*, 9–18.
(20) Pometun, M. S.; Chekmenev, E. Y.; Wittebort, R. J. *J. Biol. Chem.* **2004**, *279*, 7982–7987.
(21) Reif, B.; Xue, Y.; Agarwal, V.; Pavlova, M. S.; Hologne, M.; Diehl, A.; Ryabov, Y. E.; Skrynnikov, N. R. *J. Am. Chem. Soc.* **2006**, *128*, 12354–12355.
(22) Tamura, A.; Matsushita, M.; Naito, A.; Kojima, S.; Miura, K. I.; Akasaka, K. *Protein Sci.* **1996**, *5*, 127–139.
(23) Ying, W. W.; Irvine, S. E.; Beekman, R. A.; Siminovitch, D. J.; Smith, S. O. *J. Am. Chem. Soc.* **2000**, *122*, 11125–11128.
(24) Cutajar, M.; Lewis, M. H.; Wimperis, S. *Chem. Phys. Lett.* **2007**, *449*, 86–91.
(25) Brewer, S. H.; Vu, D. M.; Tang, Y. F.; Li, Y.; Franzen, S.; Raleigh, D. P.; Dyer, R. B. *Proc. Natl. Acad. Sci. U.S.A.* **2005**, *102*, 16662–16667.
(26) Buscaglia, M.; Kubelka, J.; Eaton, W. A.; Hofrichter, J. *J. Mol. Biol.* **2005**, *347*, 657–664.
(27) De Mori, G. M. S.; Colombo, G.; Micheletti, C. *Proteins: Struct., Funct., Bioinf.* **2005**, *58*, 459–471.
(28) Havlin, R. H.; Tycko, R. *Proc. Natl. Acad. Sci. U.S.A.* **2005**, *102*, 3284–3289.
(29) Kubelka, J.; Chiu, T. K.; Davies, D. R.; Eaton, W. A.; Hofrichter, J. *J. Mol. Biol.* **2006**, *359*, 546–553.
(30) Kubelka, J.; Eaton, W. A.; Hofrichter, J. *J. Mol. Biol.* **2003**, *329*, 625–630.
(31) McKnight, C. J.; Doering, D. S.; Matsudaira, P. T.; Kim, P. S. *J. Mol. Biol.* **1996**, *260*, 126–134.
(32) Ripoll, D. R.; Vila, J. A.; Scheraga, H. A. *J. Mol. Biol.* **2004**, *339*, 915–925.
(33) Tang, Y. F.; Goger, M. J.; Raleigh, D. P. *Biochemistry* **2006**, *45*, 6940–6946.
(34) van der Spoel, D.; Lindahl, E. *J. Phys. Chem. B* **2003**, *107*, 11178–11187.
(35) Vugmeyster, L.; Trott, O.; McKnight, C. J.; Raleigh, D. P.; Palmer, A. G. *J. Mol. Biol.* **2002**, *320*, 841–854.
(36) Wang, M. H.; Tang, Y. F.; Sato, S. S.; Vugmeyster, L.; McKnight, C. J.; Raleigh, D. P. *J. Am. Chem. Soc.* **2003**, *125*, 6032–6033.
(37) Wickstrom, L.; Bi, Y.; Hornak, V.; Raleigh, D. P.; Simmerling, C. *Biochemistry* **2007**, *46*, 3624–3634.
(38) Vugmeyster, L.; McKnight, C. J. *Biophys. J.* **2008**, *95*, 5941–5950.
(39) Bretscher, A.; Weber, K. *Cell* **1980**, *20*, 839–847.
(40) Friederich, E.; Vancompernolle, K.; Louvard, D.; Vandekerckhove, J. *J. Biol. Chem.* **1999**, *274*, 26751–26760.
(41) Chiu, T. K.; Kubelka, J.; Herbst-Irmer, R.; Eaton, W. A.; Hofrichter, J.; Davies, D. R. *Proc. Natl. Acad. Sci. U.S.A.* **2005**, *102*, 7517–7522.
(42) McKnight, C. J.; Matsudaira, P. T.; Kim, P. S. *Nat. Struct. Biol.* **1997**, *4*, 180–184.

(quadrupolar order) relaxation, that are sensitive to much faster time scales.[4] The experiments are performed over the temperature range of 112 K to 298 K. We then use computational techniques to develop appropriate motional models that describe the dynamical behavior of HP36's core in this wide temperature range.

Materials and Methods

Sample Preparation. Powdered 5,5,5-d_3 FMOC-leucine with water content of 400 ppm was purchased from Cambridge Isotopes Laboratories (Andover, MA). The HP36 sample was synthesized commercially by solid-state peptide synthesis at Biopeptide Co., Inc., San Diego, CA, with incorporation of 5,5,5-d_3 leucine at position number 69. The sample was purified by reverse-phase HPLC. The identity and purity of the sample was confirmed by mass spectroscopy and reverse-phase HPLC. Lyophilized powder (20 mg) was exposed to vapor diffusion in a desiccator until water content reached ~40% by weight, as quantified gravimetrically. Since internal dynamics on ms-μs time scale can have a strong hydration dependence,[6,22,43] it is important to choose a suitable level of hydration at which the protein is fully hydrated on one hand, and, on the other hand, the overall molecular tumbling is not reintroduced to an appreciable extent. The hydration level of ~38% corresponds roughly to one layer of water molecules and is a typical threshold at which most globular proteins are fully hydrated.[44,45] Since the sample is not crystalline, we did not add any cryoprotectant. This allows us to measure unperturbed motional parameters as a function of temperature.

Deuteron Solid-State NMR Spectroscopy. Experiments were performed at 11.7 and 17.6 T magnetic fields. A 17.6 T WB750 Bruker spectrometer, equipped with AVANCE I electronics and a static probe operating in the range of temperatures between 145 K and 380 K, was used at the College of William and Mary. A 11.7 T WB Varian Unity Plus spectrometer at Pacific Northwest National Laboratory was equipped with a MAS probe operating in the range of temperatures between 180 K and 350 K, and a static cryogenic helium-cooled probe[46] for temperatures between 4 K and 170 K.

Line shape experiments were performed with a quadrupole echo pulse sequence with an eight-step phase cycle and a delay of 31 μs between 90° pulses. (The durations of 90° pulses were 3.5 μs on the 11.7 T spectrometer and 2.0 μs on the 17.6 T spectrometer). Data acquisition was initiated prior to the echo maximum. The number of scans for the HP36 sample varied from 16384 to 32768, depending on temperature. Higher temperatures required more scans because of the lower signal-to-noise ratio. For FMOC-Leu 1024 scans were sufficient. Time domain data were left-shifted and apodized with 500 Hz exponential broadening for FMOC-Leu and 1000 Hz broadening for HP36. T_{1Z} and T_{1Q} measurements were performed by the inversion recovery and broadband Jeener−Broekaert pulse sequences, respectively, using quadrupolar echo detection schemes.[47,48] Number of scans varied between 7168 to 10240. Six to eight relaxation delays were typically used, except for the 283 K T_{1Z} data set for which 14 delays were collected. Signal intensities for the T_{1Z} experiment were taken as the sum of intensities for the two transitions of the deuteron spins and as a difference of the intensities for T_{1Q}.[3,47] Relaxation times were obtained by fitting the signal intensities at selected frequencies of the spectra as a function of relaxation delays to the monoexponential inversion recovery for T_{1Z} and monoexponential decay function for T_{1Q}. The errors in the rates were estimated by the asymptotic covariance matrix method.[49] In addition, at 233 K, 203 K, and 159 K the T_{1Z} experiments were performed on two occasions with the 17.6 T spectrometer, and the values of T_{1Z} fell within the error limits obtained by the covariance matrix method.

On the 11.7 T spectrometer, MAS probe sample temperature was calibrated using lead nitrate with 2 kHz MAS spinning.[50] On the 17.6 T spectrometer, temperature calibration was done by recording static lead nitrate line shapes[51] and using the freezing point of D_2O, 3.8 °C, as the fixed point for the calibration. The cryogenic probe on the 11.7 T spectrometer had a temperature sensor in immediate proximity to the sample area. Its reading was taken as the sample temperature.

Modeling. 1. Deuteron Line Shapes. Theoretical discussions and computational approaches for computing deuteron line shapes have been presented elsewhere.[3,52,53] A brief overview necessary for the implementation of our model is presented below. For a given orientation of a crystallite the time-domain response of the system $M(t) = M_+(t) + M_-(t)$ in a quadrupolar-echo deuterium line shape experiment is governed by

$$\frac{dM_\pm}{dt} = A_\pm M_\pm \tag{1}$$

where $\pm$ corresponds to $m = -1$ to $m = 0$ and $m = 0$ to $m = +1$ transitions of the deuteron spin. The response depends on the quadrupolar tensor orientation for each spin in the crystal-fixed frame and on the orientation of the crystallite in the laboratory frame. When orientations of the deuteron electric field gradient tensors in the crystal-fixed frame are specified by N "structural sites", i.e., N sets of three Euler angles, and the deuteron dynamics is described by Markovian jumps among sites, M becomes a multidimensional vector with the components M_i ($i = 1,.. ., N$) and A takes the form of a $N \times N$ matrix with elements

$$A_\pm^{ij} = \pm i\omega_i\delta_{ij} + K_{ij} \tag{2}$$

where i and j denote structural sites, ω_i is the orientation-dependent frequency of each site, δ is a Kronecker symbol, and K is a matrix of site-exchange rates (which does not depend on crystallite orientations). The matrix K satisfies the following two constraints: $K_{ii} = -\sum_{j=1,j\neq i}^{N} K_{ji}$, and the microscopic reversibility condition given by $K_{ij}p_j^{eq} = K_{ji}p_i^{eq}$, where p_i^{eq} is the equilibrium population of site i and K_{ij} is the rate of jumps from site j to site i. The orientation dependence of the frequencies ω_i can be expressed by

$$\omega_i = C_q \sum_{a=-2}^{2} \left(D_{0,a}^{(2)}(\Omega_{PC,i}) + \frac{\eta}{\sqrt{6}}\left(D_{2,a}^{(2)}(\Omega_{PC,i}) + D_{-2,a}^{(2)}(\Omega_{PC,i})\right)\right) D_{a,0}^{(2)}(\Omega_{CL}) \tag{3}$$

where C_q is the quadrupolar coupling constant given by $C_q = 3/4e^2qQ/\hbar$, η is the asymmetry parameter, and $D^{(2)}$ are the second-order Wigner rotation matrices defining the transformations from the principal axis frame (PAS) of the quadrupolar tensor to the crystal-fixed frame with the relative orientations given by the Euler angles $\Omega_{PC,i}$ and from the crystal-fixed frame to the laboratory frame with the relative orientations given by Euler angles Ω_{CL}. In a polycrystalline sample, the line shape is average over all possible orientations:

(43) Wang, A. C.; Kennedy, M. A.; Reid, B. R.; Drobny, G. P. *J. Magn. Reson. Ser. B* **1994**, *105*, 1–10.
(44) Rupley, J. A.; Gratton, E.; Careri, G. *Trends Biochem. Sci.* **1983**, *8*, 18–22.
(45) Khodadadi, S.; Pawlus, S.; Sokolov, A. P. *J. Phys. Chem. B* **2008**, *112*, 14273–14280.
(46) Lipton, A. S.; Heck, R. W.; Sears, J. A.; Ellis, P. D. *J. Magn. Reson.* **2004**, *168*, 66–74.
(47) Hoatson, G. L. *J. Magn. Reson.* **1991**, *94*, 152–159.
(48) Wimperis, S. *J. Magn. Reson.* **1990**, *86*, 46–59.
(49) Shao, J. *Mathematical Statistics*; Springer: New York, 2003.
(50) Neue, G.; Dybowski, C. *Solid State Nucl. Magn. Reson.* **1997**, *7*, 333–336.
(51) Beckmann, P. A.; Dybowski, C. *J. Magn. Reson.* **2000**, *146*, 379–380.
(52) Torchia, D. A.; Szabo, A. *J. Magn. Reson.* **1982**, *49*, 107–121.
(53) Vold, R. L.; Hoatson, G. L. *J. Magn. Reson.* **2009**, *198*, 57–72.

$$I(\omega) = \int d\Omega_{CL} \mathrm{Re} \int dt \sum_i (M_{+,i}(t) + M_{-,i}(t)) e^{-i\omega t} \quad (4)$$

Simulated data were generated using the MATLAB program EXPRESS,[53] which solves eq 1 and performs the integration of eq 4 by tiling algorithms that optimize the set of crystallite orientations. The input includes user-defined matrices K_{ij}, PAS tensor orientations for each jump site, and populations for each site. Different motional modes are input with respect to different, easy to visualize coordinate frames with separate input parameters. EXPRESS then computes and displays an equivalent one-frame representation which is used in further computations.

Line shapes were fit to a three-mode motional model depicted in Figure 2. Here, the first mode of motion corresponds to fast three-site hops of the methyl deuterons with the rate matrix K_{ij}^{methyl}, the second mode approximates diffusion of the $C^{\gamma}-C^{\delta}$ axis on a restricted arc with rate matrix K_{ij}^{arc}, and the third mode models large angle rotameric jumps with rate matrix K_{ij}^{rot}. Each of the modes is represented by a separate frame in EXPRESS.

For the purpose of line shape simulations in the temperature range of our experiments, the three-site hops of the CD_3 groups are fast enough to produce a single effective axially symmetric quadrupolar tensor (directed along the $C^{\gamma}-C^{\delta}$ axis) with an effective quadrupolar constant C_q*. This approximation allows us to run the simulations using only the second and third frames instead of including all three frames explicitly.

In the second frame the $C^{\gamma}-C^{\delta}$ axis moves on the arc of a cone with apex angle 141° as defined by the tetrahedral geometry. We assume without loss of generality that the $C^{\gamma}-C^{\delta}$ axis has a preferred direction in the crystal-fixed frame corresponding to $\varphi = 0$, where φ is the azimuthal angle in a spherical coordinate system associated with the C^{γ} atom and the $C^{\beta}-C^{\gamma}$ bond lies on the polar axis. The arc itself is represented by several sites with values of φ incremented in $\Delta\varphi = 5°$ steps. For example, a 30° arc is given by seven sites with $\varphi = -15°$ to $\varphi = 15°$. The effective diffusion coefficient D is given by

$$D = \Delta\phi^2 k \quad (5)$$

where $k = K_{i,i+1}^{\mathrm{arc}} = K_{i+1,i}^{\mathrm{arc}}$ is the jump rate between two neighboring sites in the arc frame. Only nearest-neighbor jumps are allowed. A similar approach has been used by Meints et al.[54] to describe local motions in solid deoxyribonucleic acids.

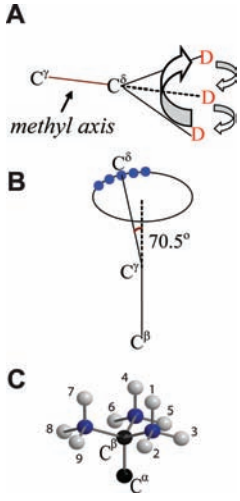

Figure 2. Schematic representation of the motional model which is used to fit the line shape data for L69 in HP36. The first mode (A) corresponds to fast three-site hops of the methyl group; the second mode (B) corresponds to a restricted diffusion on an arc approximated by small nearest neighbor jumps of the $C^{\gamma}-C^{\delta}$ axis; the third mode (C) corresponds to the configuration of nine possible rotamers in the leucine side chain. Nine possible positions of C^{δ} atoms are shown in gray, and three possible positions of C^{γ} are shown in blue. The following configurations have the same orientations: 1, 4, 7; 2, 9; 3, 5; 6, 8.

The third frame corresponds to four different orientations of $C^{\beta}-C^{\gamma}$ axis which point at the four vertices of a tetrahedron. This gives a four-site frame where the populations of the sites can be different and jumps are allowed between each pair of sites. We use a model with x:1:1:1 ratios of populations at the four sites.

In order to find the parameters corresponding to experimental line shapes, we have generated libraries of spectra using ranges of input parameters that give spectral shapes visually similar to experimental data. The variable parameters were arc length, diffusion rate along the arc, and jump rate in the rotameric frame. In a search for the parameters of the model that give the best fit to the experimental spectra, our goal was 2-fold. First, we tried to minimize the overall difference between experimental and simulated spectra $\Delta s = \int (I^{\mathrm{exp}}(\omega) - I^{\mathrm{sim}}(\omega))^2 d\omega$, where both simulated and experimental spectra are normalized in such a way that the horn height equals 1. Second, we tried to match the distance between the horns. To do that, we minimized the square of the difference between experimental and simulated horn distances, Δh. These two minimizations lead to somewhat different model parameters. We, therefore, decided to minimize a combined function, where both criteria would play an equal role:

$$\tilde{\chi}^2 = \frac{\Delta s}{\Delta s^* - \Delta s_{\mathrm{min}}} + \frac{\Delta h}{\Delta h^* - \Delta h_{\mathrm{min}}} \quad (6)$$

Here Δs_{min} and Δh_{min} are minimum values of Δs and Δh, respectively, Δs^* is the value of Δs calculated for the parameters that minimize Δh, and Δh^* is the value of Δh calculated for the parameters that minimize Δs.

2. Relaxation Data. Zeeman T_{1Z} and quadrupolar order T_{1Q} relaxation rates are given by[4,5]

$$\frac{1}{T_{1Z}} = \frac{3\pi^2}{2} C_q^2 (J_1(\omega_0) + 4J_2(2\omega_0))$$
$$\frac{1}{T_{1Q}} = \frac{9\pi^2}{2} C_q^2 J_1(\omega_0), \quad (7)$$

where ω_0 is the Larmor frequency, J_1 and J_2 are spectral density functions, and C_q refers to the quadrupole coupling constant (units are hertz) in the absence of motion. J_1 and J_2 are dependent on time scales and type of underlying motional processes, as well as on crystallite orientations. The dependence on the crystallite orientation is unique for each motional model, and thus the anisotropies in the relaxation rates can be useful in discriminating among several motional models. Spectral density functions can be obtained analytically for several simple models of motion.[52] However, motional models with multiple modes usually require computer simulations.

EXPRESS was used to simulate relaxation rates for the three-mode motional model depicted in Figure 2. The three-site jumps are defined in the first frame and the arc motion in a second frame, while a third frame is used to define the rotameric jumps. For each temperature, parameters of the arc motion and rotameric jumps were fixed at values determined using the line shape data. Then, for each temperature a library of the relaxation rates was created as a function of the three-site hop rate, k^{methyl}.

As explained later in Results and Discussion, relaxation data are best fitted by a model with the existence of a crossover temperature T*, such that the three-site hop rates follow an Arrhenius law with different activation energies above and below T*. For temperatures above T*, a Gaussian distribution of the activation energies is needed to fit the data. When $T < T$*, a single value of the activation energy was sufficient. Within this model the continuity of the

(54) Meints, G. A.; Miller, P. A.; Pederson, K.; Shajani, Z.; Drobny, G. *J. Am. Chem. Soc.* **2008**, *130*, 7305–7314.

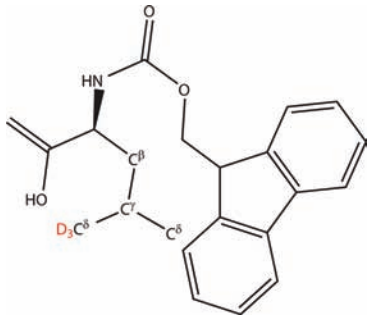

Figure 3. Structure of 5,5,5-d_3 FMOC-Leu with one of the labeled sites shown in red. $C^{\delta 1}$ and $C^{\delta 2}$ methyl groups are labeled in 50%/50%.

relaxation rates at the crossover temperature can be approximated by the condition $\langle \ln k_{high}^{methyl}(T^*) \rangle = \ln k_{low}^{methyl}(T^*)$, where indices "high" and "low" denote the limits from the high and low temperature side and $\langle ... \rangle$ stands for the average over conformational ensemble. Thus, this procedure involves five adjustable fitting parameters: the Arrhenius law prefactor for the high temperature side, the average activation energy for $T > T^*$, the width of its Gaussian distribution σ, the activation energy for $T < T^*$, and T^* itself. For each temperature above T^*, the simulated relaxation rates were calculated as weighted averages of the relaxation rates corresponding to particular values of activation energies taken from the Gaussian distribution. Correspondence between the values of the three-site hop rates and the relaxation rates was established from the libraries described above. Below T^* a single value of activation energy was used in the calculations. The predicted rates at powder pattern horn positions were compared with the experimental values, and the best fit parameters were obtained through χ^2 minimization. The errors in fitted parameters were estimated by the covariance matrix method.[49]

Results and Discussion

5,5,5-d_3 FMOC-Leu (Figure 3), used for the solid-state peptide synthesis of HP36, has a deuteron label which is equally distributed between the two C^{δ} positions. As a result, in HP36 protein there will be roughly equal fractions of molecules with deuteron labels at either $C^{\delta 1}$ or $C^{\delta 2}$ methyls in L69. Thus, all of our line shape and relaxation measurements have contributions from both positions. Slow motions around $C^{\beta}-C^{\gamma}$ axis or rotameric jumps of the side chains affect both of the groups simultaneously and thus would yield the same parameters for the two positions. In addition, within the experimental errors the measured relaxation curves cannot be distinguished from single-exponential behavior at all temperatures, which indicates that the relaxation times and activation energies are very similar for the two sites. Magic angle spinning experiments at room temperature and static quadrupole-echo CPMG measurements at 140 K did not reveal any difference in the chemical shifts of the two C^{δ} positions for either FMOC-Leu or L69 of HP36. We thus refer to the 5,5,5-d_3 label as "single-site", keeping in mind that the data represent an average of two very similar sites.

Line Shapes Can Be Modeled with a Combination of Diffusive Motions on a Restricted Arc and Rotameric Jumps. Experimental line shapes for the HP36 sample are presented in Figure 4A. The overall spectral shapes are characteristic of fast-limit methyl group rotation. However, it is clear that at higher temperatures, additional slower motions are present on the ms-μs time scale. These additional motions lead to further narrowing of the powder pattern, accompanied by slanting of the shoulders and build-up of extra intensity in the middle of the spectra.

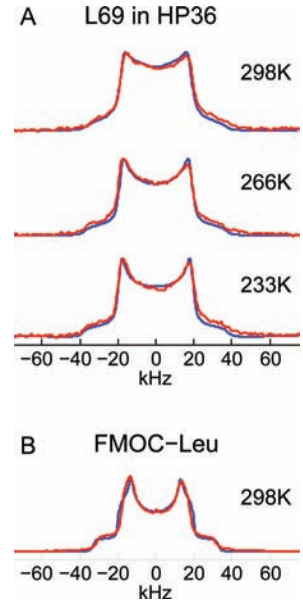

Figure 4. Experimental (red) and simulated (blue) quadrupolar echo line shapes of (A) L69 in HP36 at several temperatures and (B) 5,5,5-d_3 FMOC-Leu at 298 K.

In order to discern possible mechanisms contributing to these somewhat unusual shapes, we first looked at experimental spectra of FMOC-Leu, which is a much simpler system than the hydrophobic core of a protein but still consists of a leucine side chain in a close proximity to a bulky hydrophobic group (Figure 3). The line shape data for FMOC-Leu at 25 °C are shown in Figure 4B. The line shape at high temperatures clearly indicates the presence of a small asymmetry parameter. Motional models with either small-angle symmetric jumps of the methyl axis or an axially symmetric rotation about the methyl axis cannot reproduce the observed asymmetry. A simple model which is consistent with the molecular geometry and introduces a small asymmetry is diffusion on a restricted arc illustrated in Figure 2B. A spectrum simulated according to this model is shown in Figure 4B and gives a very good fit to the experimental leucine line shape with the arc length of 70° and the diffusion coefficient of 1.1×10^5 rad^2/s.

Compared to Fmoc-Leu data (Figure 4B), the spectra for HP36 (Figure 4A) show more intensity in the middle and more slanted, rounded shoulders. The restricted arc motion by itself is not enough to explain these line shapes. Our simulations show that incorporation of additional large angle jump motion does account adequately for these features. Also, detailed comparison with the FMOC-Leu data shows that for the protein, the outer edges of the horns are in fact sharper, while the shoulder-to-shoulder span is larger. This implies that diffusive asymmetric motion is of smaller amplitude in the protein than in Fmoc-Leu.

We thus arrive at the conclusion that there are two sources of slow motion in L69 of HP36. The first mode is diffusive motion of the $C^{\gamma}-C^{\delta}$ axis on a restricted arc around positions corresponding to rotameric configurations of the L69 side chain. The second mode is due to large angle jumps between rotamers. In general, a leucine side chain can assume nine rotameric configurations (shown in Figure 2C) characterized by dihedral angles of rotations around $C^{\alpha}-C^{\beta}$ and $C^{\beta}-C^{\gamma}$ bonds, χ_1 and χ_2

respectively.[55] Each of these angles has three possible values, 60°, 180°, and 300°. The combined effect of these two rotations leads to four possible orientations of $C^{\gamma}-C^{\delta}$ axis, pointing in the directions toward four vertices of a tetrahedron.[56,15]

However, X-ray and NMR structures of HP36[41,42] show only one major rotameric conformation for L69 which corresponds to $\chi_1 = 300°$, $\chi_2 = 180°$. Our fitting parameters for the second mode should therefore be consistent with this conclusion by using nonequal population of rotamers for this mode.

To describe the contribution from the minor rotameric configurations, we first attempted a two-conformer model for large angle rotameric jumps. The resulting line shapes overestimated the asymmetry parameter (see Figure S1). We therefore chose a four-conformer model, which allows for all possible orientations of $C^{\gamma}-C^{\delta}$ axis. Since the $C^{\gamma}-C^{\delta}$ axis is already involved in the motion along a restricted arc, we simulated the rotameric jumps by allowing the $C^{\beta}-C^{\gamma}$ axis to point toward four vertices of a tetrahedron. In the absence of the motion along the arc, this would lead to the same geometric configuration for the $C^{\gamma}-C^{\delta}$ axis as in the real nine rotamers. In the presence of the arc mode motion, this is a reasonable approximation, allowing us to keep the number of fitting parameters to a necessary minimum.

We assumed equal populations for three minor conformers. Populations were fitted only at the highest temperature of 25 °C with the values of 84.3% for one (major) form and a total of 16.7% for all three minor forms, which corresponds to the energy difference of 6.7 kJ/mol. For other temperatures we varied the relative populations of major and minor forms according to the Boltzmann law. The effective value of the quadrupole constant C_q* was taken as 53.3 ± 0.1 kHz, which is given by the quadrupolar splitting at the lowest temperature, 112K.

Spectra simulated according to the discussed model of motion are shown by solid blue lines in Figure 4A for several temperatures between 298−233 K and give excellent fits to the data. Best fits were obtained for all temperatures with the same arc length, 30°, and a temperature-independent rate for the rotameric jumps $k^{rot} = 4 \times 10^4$ s^{-1}. The rates of restricted diffusion varied with temperature (see Table S1). Diffusion coefficients calculated from the best fit jump rates according to eq 5 are shown in Figure 6 on an Arrhenius plot. The activation energy is 37 kJ/mol. This large value implies that the restricted diffusional motion sets in only at relatively high temperature. At temperatures below 233 K there is almost no change in the horn distances, and the spectra are not very sensitive to the diffusion rates.

Figure 5 shows $\tilde{\chi}^2$ contour plots for HP36 at 25° obtained as a result of the minimization procedure described by eq 6. Note the correlation between the influences of the diffusion coefficient and rotameric jumps rate on the quality of the fit. Also, the dependence of $\tilde{\chi}^2$ on the diffusion coefficient is asymmetric; the contours are a lot denser on the side of the smaller diffusion coefficients. This indicates that the motion along the arc is approaching the fast limit.

The motional model developed above allows for the calculation of the order parameter of slow motions S^2_{slow}, characterizing the amplitude of fluctuations of leucine side chain on the μs-ms time scale. Order parameters calculated on the basis of

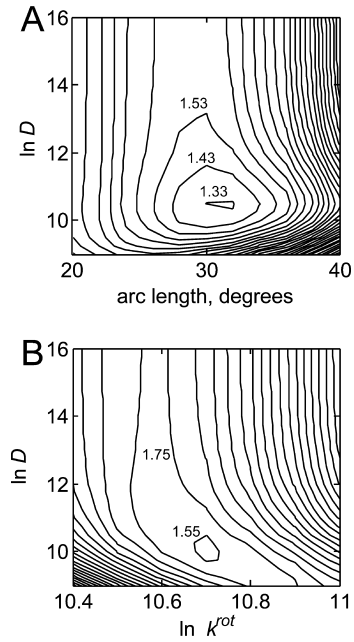

Figure 5. $\tilde{\chi}^2$ plots for (a) arc length and diffusion coefficient for the restricted diffusion on the arc with contour levels shown in 0.1 steps, and (b) diffusion coefficient for the restricted diffusion on the arc and the rate of rotameric jumps with contour levels shown in 0.2 steps.

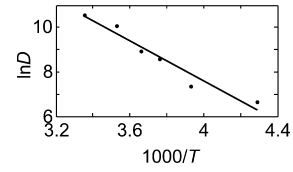

Figure 6. Arrhenius plot of diffusion coefficients for the arc motion mode in L69 of HP36. Solid line corresponds to a linear fit.

motional models obtained from solid-state NMR line shapes in principle can be compared to the values extracted from residual dipolar coupling experiments. Thus, they can provide a means for comparison of solution and solid-state dynamics of proteins.[14] The details of calculations of S^2_{slow} and its temperature dependence are presented in the Supporting Information.

Note that the order parameters define experimental line shapes only when motions are in the fast limit and do not induce an apparent asymmetry parameter in the motionally averaged quadrupole coupling tensor. In our case, the time scale of slow modes of motion corresponds to intermediate regime, and we do have an effective asymmetry parameter. As a result, the experimental line shapes cannot be fully characterized in terms of order parameters, and explicit motional modeling is necessary.

An alternative approach for line shape modeling would be the use of an angular harmonic potential for the restricted diffusion on the arc mode.[54] We have considered the use of such a potential, which leads to nonequal populations along the arc. However, the line shapes derived from such a model with the populations constrained by the Boltzmann law failed to adequately fit the experimental line shape data. More details regarding the simulation according to this model are available in the Supporting Information (Figure S2).

In addition to line shape simulations, we have examined T_{1Z} anisotropy profiles to provide further support of our motional model.[4,52] Figure 7 shows a detailed analysis of the anisotropy profile at 10 °C, where sufficient signal-to-noise ratio was achieved to define T_{1Z} times across all frequencies. First, the

(55) Janin, J.; Wodak, S.; Levitt, M.; Maigret, B. *J. Mol. Biol.* **1978**, *125*, 357–386.
(56) Huang, T. H.; Skarjune, R. P.; Wittebort, R. J.; Griffin, R. G.; Oldfield, E. *J. Am. Chem. Soc.* **1980**, *102*, 7377–7379.

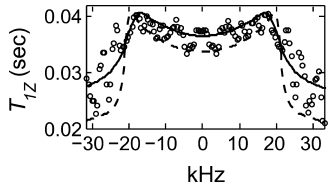

Figure 7. T_{1Z} relaxation anisotropy profiles at 10 °C and 17.6 T for L69 in HP36. Experimental data (circles) are compared to the simulated profile according to the three-site hops mode (dotted line), and the full three-mode motional model described in text (solid line).

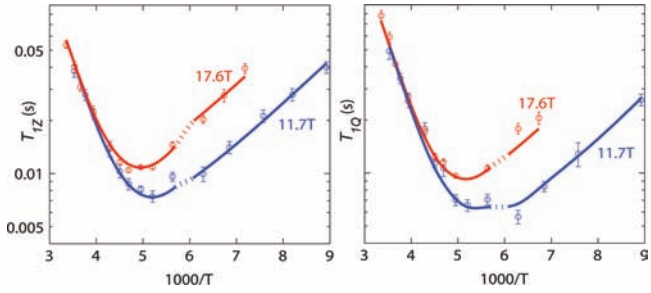

Figure 8. Semilog plots of T_{1Z} and T_{1Q} relaxation times at horn positions versus 1000/T at 17.6 T (red circles) and 11.7 T (blue circles). Simulated data (solid lines) were generated according to the phenomenological model described in the text. Dotted line indicates the crossover region.

existence of observable anisotropy supports the model of three-site hops about the methyl spinning axis, as opposed to rotation diffusion, in agreement with earlier works.[57] However, the magnitude of the anisotropy is smaller than that predicted for three-site hops alone (shown by dotted line in Figure 7). The addition of slow motional modes reduces the magnitude of the anisotropy for the simulated rates (shown by solid line), bringing them into agreement with the experimental data.

The line shape data for the HP36 sample labeled at a single site allowed for a unique opportunity for a very detailed investigation of the mechanisms leading to μs-ms time scale dynamics of a buried methyl group. Unlike the rotameric mode, which is widely used in conjunction with the three-site hops in the interpretation of motional order parameters resulting from solution NMR measurements,[14,21,58−61] models based on restricted diffusive motion are not often discussed (see, however, Daragan and Mayo[62]).

Relaxation Data Reflects Changes in the Local Environment of L69. T_{1Z} and T_{1Q} relaxation times at the horn positions are presented in Figure 8 as a function of temperature. Fast three-site hops of C^{δ} methyl groups in leucine side chains, depicted in Figure 2a, occur on the picosecond time scale in this temperature regime and are usually thought to be the main contribution to the relaxation rates. Two features are immediately apparent looking at the relaxation times in Figure 8. First, if we were to describe the relaxation assuming three-site hops with a *single* activation energy (shown in Supporting Information Figure S3), the minima would be roughly 40% smaller in magnitude and much sharper. Second, the slopes on both sides of the minima are markedly different, again contradicting the simple mechanism just described.

These experimental features led us to consider the following phenomenological model. We fit the data with two different Arrhenius activation energies and an effective crossover temperature. The quality of the fit is greatly improved when a Gaussian distribution of activation energies is used on the high-temperature side of the relaxation curve. Interestingly, the use of a distribution on the low-temperature side does not change the quality of the fit. Thus, the origin of the distribution is likely to stem from a conformational ensemble present in the protein. The number of available conformations is greatly decreased at low temperatures.

In addition to the three-site methyl hops, all simulations included restricted diffusion on the arc, as well as rotameric jumps between traces of minor rotameric conformers that gave 3−9% contribution to the overall relaxation rates. The model gives an excellent fit to the experimental results with the following values of the fitted parameters. Above the crossover temperature of $T^* = 170.1 \pm 1.6$ K the value of the activation energy is 14.4 ± 0.2 kJ/mol, the width of the Gaussian distribution is 1.63 ± 0.05 kJ/mol, and the prefactor is $(2.1 \pm 0.2) \times 10^{12}$ s^{-1}. Below T^* the activation energy is 4.7 ± 0.2 kJ/mol. Relaxation times simulated according to the above model are shown by solid lines in Figure 8. In reality the crossover is likely to occur within a narrow temperature range rather than at one specific point. To stress this point, we show the crossover region by a dotted line in Figure 8. Since both T_{1Z} and T_{1Q} relaxation times can be fitted with the same crossover temperature at two different NMR field strengths, our data suggest that the crossover has a physical origin independent of the models used to fit the NMR relaxation data.

Modern technology allows for the use of magic angle spinning techniques at temperatures down to 25 K.[63] Thus, in principle one could conduct a similar study for multiple sites with site-specific resolution. However, special thought will have to be given to the treatment of spin-diffusion effects arising as the result of the introduction of multiple deuteron labels.[24] Moreover, MAS suppresses anisotropy in the measurements of T_{1Z} and T_{1Q}, so this source of dynamic information would be lost if MAS is used to achieve site-specific resolution.

The high-temperature value of the activation energy is within the range typical for methyl groups in other proteins.[64] The low-temperature value is three times lower. This drastic change in the slope on the lower temperature side of the minima suggests that the local environment around the L69 side chain undergoes a remarkable transformation at T^*. The slope on the low temperature side is smaller, indicating that the barrier for methyl rotation is decreased. Thus, at temperatures below T^*, the C^{δ} deuterons of L69 become more free to rattle inside a "cage" that constrained their motions at higher temperatures.

A variety of factors could provoke this behavior, such as changes in backbone dynamics or other, more local effects inside the core. For example, the neighboring ring of F58 could experience dynamic conformational changes in such a way as to "free" the environment around L69.A recent study by Bajaj et al.[65] on model peptides supports the idea that the change in

(57) Batchelder, L. S.; Niu, C. H.; Torchia, D. A. *J. Am. Chem. Soc.* **1983**, *105*, 2228–2231.
(58) Igumenova, T. I.; Frederick, K. K.; Wand, A. J. *Chem. Rev.* **2006**, *106*, 1672–1699.
(59) Tugarinov, V.; Kay, L. E. *Chembiochem.* **2005**, *6*, 1567.
(60) Hu, H.; Hermans, J.; Lee, A. L. *J. Biomol. NMR* **2005**, *32*, 151–162.
(61) Chou, J. J.; Case, D. A.; Bax, A. *J. Am. Chem. Soc.* **2003**, *125*, 8959–8966.
(62) Daragan, V. A.; Mayo, K. H. *Prog. Nucl. Magn. Reson. Spectrosc.* **1997**, *31*, 63–105.
(63) Thurber, K. R.; Tycko, R. *J. Magn. Reson.* **2008**, *195*, 179–186.
(64) Xue, Y.; Pavlova, M. S.; Ryabov, Y. E.; Reif, B.; Skrynnikov, N. R. *J. Am. Chem. Soc.* **2007**, *129*, 6827–6838.
(65) Bajaj, V. S.; van der Wel, P. C. A.; Griffin, R. G. *J. Am. Chem. Soc.* **2009**, *131*, 118–128.

the methyl environment of L69 in HP36 may be caused by changes in the dynamics of the neighboring phenylalanine ring. This and other possible causes of the change in the apparent activation energy barrier will be a subject of future investigation.

Although our experiment is conducted on a local probe and, therefore, cannot fully elucidate global changes experienced by the protein, we would like to discuss the place of the observed crossover phenomenon in the emerging scheme of the dynamic changes occurring with the proteins at low temperatures.

It is well-known that proteins exhibit a so-called protein glass-transition, i.e., a dynamic transition occurring at about 200−230 K leading to a loss of biological activity.[66,67] X-ray diffraction, neutron scattering studies, and dielectric spectroscopy, as well as evidence from NMR relaxation measurements, indicate freezing of slow collective modes of motion below the transition temperature.[68−75] Various arguments have been presented that connect the transition to solvent participation.[66,70,75−77] In addition to the solvent-related modes that are frozen below the glass-transition temperature, there are anharmonic motions at temperatures below 200 K which are likely to be dominated by methyl group dynamics down to about 100 K.[71,74,67] The observed crossover phenomenon reported here may be highlighting characteristics of the latter internal modes.

Conclusions

We investigated the dynamics of the hydrophobic core of a hydrated HP36 sample by looking at the $C^{\delta}D_3$ groups of L69 located in the key position of the core. Deuteron line-shape analysis over a wide range of temperatures led to a three-mode motional model. Besides three-site hops which are in the fast limit, additional slower motions are present that can be attributed to two different sources. The first one can be described by diffusion along a restricted arc of about 30° modeled by nearest-neighbor jumps, and the second one by large angle jumps between traces of rotamers.

The temperature-dependence of the relaxation rates shows two features: a non-Arrhenius behavior with broadened minimum and a distinct decrease in the value of the apparent activation energy on the low temperature side. We fit the data using a phenomenological model where a Gaussian distribution of activation energies with the average value of 14.4 kJ/mol collapses to a single very different value of 4.7 kJ/mol at around 170 K. The necessity of the distribution exclusively on the high temperature side reflects the heterogeneity of the folded conformational ensemble at higher temperatures. The drastic decrease in the value of the activation energy on the lower temperature side stems from changes in the local environment of the L69 side chain.

The combination of deuteron NMR line shape analysis and relaxation data over a wide temperature range provided stringent constraints on the choice of motional models. Our results thus indicate that single-site labeling of methyl groups in conjunction with the NMR experiments allows for detailed investigations of structural and dynamic characteristics of proteins hydrophobic cores.

Acknowledgment. Part of this research was performed using EMSL, a national scientific user facility sponsored by the Department of Energy's Office of Biological and Environmental Research located at Pacific Northwest National Laboratory. NMR data at 17.6 T were collected at the College of William and Mary NMR laboratory, which is supported by NSF Grant CHE-0713819 to the College of William and Mary on behalf of R.L.V. and G.L.H. L.V. is supported by the University of Alaska funds 104110-11970&11470 and Environment and Natural Resources Institute, University of Alaska at Anchorage. We are grateful to Jesse Sears, Christopher A. Maher, and Peter J. de Castro for technical assistance and to Dr. Paul Ellis for useful discussions.

Supporting Information Available: Figure S1. Line shapes simulated according to the two-site rotameric jumps mode to be compared with the four-site jumps mode. Figure S2. Line shapes simulated according to the angular harmonic potential model for the restricted diffusion on the arc. Figure S3. Comparison of the relaxation data with the three-site hops model. Table S1a. Experimental line shape parameters. Table S1b. Fitted rates of the restricted diffusion mode. Table S2. Correlation matrices for the five fitting parameters which were used to fit the relaxation data. Order parameter for slow motional modes. This material is available free of charge via the Internet at http://pubs.acs.org.

JA902977U

(66) Ringe, D.; Petsko, G. A. *Biophys. Chem.* **2003**, *105*, 667–680.
(67) Doster, W. *Eur. Biophys. J.* **2008**, *37*, 591–602.
(68) Baysal, C.; Atilgan, A. R. *Biophys. J.* **2002**, *83*, 699–705.
(69) Goddard, Y.; Korb, J.-P.; Bryant, R. G. *J. Chem. Phys.* **2007**, *126*, 175105.
(70) Goddard, Y. A.; Korb, J. P.; Bryant, R. G. *Biophys. J.* **2006**, *91*, 3841–3847.
(71) Lee, A. L.; Wand, A. J. *Nature* **2001**, *411*, 501–504.
(72) Papadopoulos, P.; Floudas, G.; Schnell, I.; Klok, H. A.; Aliferis, T.; Iatrou, H.; Hadjichristidis, N. *J. Chem. Phys.* **2005**, *122*, 224906.
(73) Doster, W. *Phys. B* **2006**, *385−86*, 831–834.
(74) Roh, J. H.; Novikov, V. N.; Gregory, R. B.; Curtis, J. E.; Chowdhuri, Z.; Sokolov, A. P. *Phys. Rev. Lett.* **2005**, *95*, 038101.
(75) Vitkup, D.; Ringe, D.; Petsko, G. A.; Karplus, M. *Nat. Struct. Biol.* **2000**, *7*, 34–38.
(76) Best, R. B.; Clarke, J.; Karplus, M. *J. Am. Chem. Soc.* **2004**, *126*, 7734–7735.
(77) Miyazaki, Y.; Matsuo, T.; Suga, H. *J. Phys. Chem. B* **2000**, *104*, 8044–8052.